Earth's Future

RESEARCH ARTICLE
10.1029/2021EF002634

Increased Global Vegetation Productivity Despite Rising Atmospheric Dryness Over the Last Two Decades

Yang Song[1,2], Wenzhe Jiao[2], Jing Wang[1], and Lixin Wang[2]

[1]College of Resources and Environmental Sciences, China Agricultural University, Beijing, China, [2]Department of Earth Sciences, Indiana University-Purdue University Indianapolis, Indianapolis, IN, USA

Key Points:

- Multiple lines of evidence showed that global vegetation productivity has increased significantly over the last two decades
- We quantified the relative impacts of vapor pressure deficit (VPD), temperature, and atmospheric CO_2 concentration on solar-induced chlorophyll fluorescence (SIF) or gross primary productivity (GPP)
- Rising VPD counteracted a small proportion of the increase in SIF (or GPP) under concurrent climate warming and CO_2 increasing

Supporting Information:

Supporting Information may be found in the online version of this article.

Correspondence to:

J. Wang and L. Wang,
wangj@cau.edu.cn;
lxwang@iupui.edu

Citation:

Song, Y., Jiao, W., Wang, J., & Wang, L. (2022). Increased global vegetation productivity despite rising atmospheric dryness over the last two decades. *Earth's Future*, *10*, e2021EF002634. https://doi.org/10.1029/2021EF002634

Received 16 JAN 2022
Accepted 13 JUN 2022

Author Contributions:

Conceptualization: Yang Song
Data curation: Yang Song
Formal analysis: Yang Song
Investigation: Yang Song
Methodology: Yang Song
Project Administration: Jing Wang, Lixin Wang
Resources: Wenzhe Jiao
Software: Yang Song
Supervision: Jing Wang, Lixin Wang
Validation: Wenzhe Jiao
Visualization: Yang Song

Abstract Rising atmospheric dryness [vapor pressure deficit (VPD)] can limit photosynthesis and thus reduce vegetation productivity. Meanwhile, plants can benefit from global warming and the fertilization effect of carbon dioxide (CO_2). There are growing interests to study climate change impacts on terrestrial vegetation. However, global vegetation productivity responses to recent climate and CO_2 trends remain to be fully understood. Here, we provide a comprehensive evaluation of the relative impacts of VPD, temperature, and atmospheric CO_2 concentration on global vegetation productivity over the last two decades using a robust ensemble of solar-induced chlorophyll fluorescence (SIF) and gross primary productivity (GPP) data. We document a significant increase in global vegetation productivity with rising VPD, temperature, and atmospheric CO_2 concentration over this period. For global SIF (or GPP), the decrease due to rising VPD was comparable to the increase due to warming but far less than the increase due to elevated CO_2 concentration. We found that rising VPD counteracted only a small proportion (approximately 8.1%–15.0%) of the warming and CO_2-induced increase in global SIF (or GPP). Despite the sharp rise in atmospheric dryness imposing a negative impact on plants, the warming and CO_2 fertilization effects contributed to a persistent and widespread increase in vegetation productivity over the majority (approximately 66.5%–72.2%) of the globally vegetated areas. Overall, our findings provide a quantitative and comprehensive attribution of rising atmospheric dryness on global vegetation productivity under concurrent climate warming and CO_2 increasing.

Plain Language Summary Earth is undergoing a sharp rise in atmospheric dryness [vapor pressure deficit (VPD)], temperature, and carbon dioxide (CO_2) concentration. Rising VPD can limit photosynthesis and thus reduce vegetation productivity. However, climate warming and CO_2 increasing can benefit vegetation productivity to some extent. Therefore, global vegetation responses to a changing climate is much more complex than expected. Here, a robust ensemble of solar-induced chlorophyll fluorescence and gross primary productivity data was used to evaluate the relative impacts of VPD, temperature, and atmospheric CO_2 concentration on global vegetation productivity over the last two decades. Our multiple lines of evidence indicated that global vegetation productivity has increased under rising VPD, temperature, and atmospheric CO_2 concentration during this period. Furthermore, we found that the negative impact of rising VPD on global vegetation productivity was comparable to the warming-induced increase but much smaller than the CO_2-induced increase. That is, rising VPD counteracted only a small proportion of the warming and CO_2-induced increase. Overall, our findings provide a quantitative and comprehensive attribution of rising atmospheric dryness on global vegetation productivity under concurrent climate warming and CO_2 increasing.

1. Introduction

Global mean annual temperature and carbon dioxide (CO_2) concentration have been on the rise since the industrial revolution (Falkowski et al., 2000), and it is expected that they will remain at high levels in the next decades (Friedlingstein et al., 2019; IPCC, 2018). In this context, terrestrial vegetation plays a vital role in mediating the relationship between climate change and carbon cycles (Le Quere et al., 2009; Randerson et al., 1997). Previous studies attributed part of the increase in vegetation productivity to the CO_2 fertilization effect, a process that acts as a negative feedback (a type of regulation to maintain stability and homeostasis in a system) for terrestrial ecosystems to resist climate change (Field et al., 2007; Friedlingstein et al., 2014; Haverd et al., 2020; Schimel et al., 2015). Moreover, global warming can enhance vegetation productivity by lengthening the active growing season and improving the maximum photosynthetic rate (Bastos et al., 2019; Myneni et al., 1997; Nemani et al., 2003; Thomas et al., 2016). The widespread increases in vegetation productivity driven by the warming and CO_2 fertilization effects have been observed across the globe (Gonsamo et al., 2021; Zhu et al., 2016). However,

Writing – original draft: Yang Song
Writing – review & editing: Wenzhe Jiao, Jing Wang, Lixin Wang

recent studies indicated that Earth is undergoing a sharp rise in atmospheric dryness as a result of the increased vapor pressure deficit (VPD) (Ficklin & Novick, 2017; Jung et al., 2010; Lopez et al., 2021; Yuan et al., 2019). Rising VPD can significantly reduce stomatal conductance and limit the actual photosynthetic rate, leading to a remarkable decline in vegetation productivity (Ding et al., 2018; Grossiord et al., 2020; He et al., 2021; Lopez et al., 2021; Novick et al., 2016; Restaino et al., 2016; Yuan et al., 2019). However, in most of the wettest parts of Amazon rainforest, vegetation photosynthesis and productivity tend to increase with rising VPD due to the changes in canopy properties (Green et al., 2020). Specifically, new leaves have higher photosynthetic capacity than the leaves they replaced in the dry season (Green et al., 2020). Besides, there is emerging evidence that vegetation productivity would receive fewer benefits from the increases in temperature and CO_2 concentration because of the global warming hiatus (Wang et al., 2019) and the decline of CO_2 fertilization effects (Penuelas et al., 2017; Wang et al., 2020; Winkler et al., 2021). Despite VPD, temperature, and atmospheric CO_2 concentration are considered as critical variables in determining vegetation productivity (Bastos et al., 2019; Fernandez-Martinez et al., 2019; Penuelas et al., 2017; Yuan et al., 2019), their actual impacts remain to be fully understood at a global scale (Green et al., 2020; Zhu et al., 2016). The relative impacts of rising VPD, temperature, and atmospheric CO_2 concentration on global vegetation productivity need to be further quantified.

The responses of terrestrial ecosystems to climate change have been well studied based on field experiments and ecosystem models. Previous findings have demonstrated that changes in VPD, temperature, and atmospheric CO_2 concentration can significantly influence plant growth by controlling photosynthetic rate, stomatal conductance, CO_2 assimilation, and other physiological pathways (Bonan et al., 2014; Green et al., 2020; Lopez et al., 2021; Piao et al., 2013; Wang et al., 2020). Moreover, the remotely sensed indicators such as Vegetation Indices (VIs) and Leaf Area Index (LAI) were used to investigate the relationships between terrestrial ecosystems and climate change at regional and global scales (Myneni et al., 1997; Nemani et al., 2003; Zhang, Song, et al., 2017; Zhu et al., 2016). Recent studies suggested that satellite-derived measurements of solar-induced chlorophyll fluorescence (SIF) can capture climate change impacts on vegetation productivity better than other indicators (Dechant et al., 2020; Fournier et al., 2012; Migliavacca et al., 2017; Song et al., 2021). SIF as a by-product of vegetation photosynthesis with a weak signal re-emitted at wavelengths of 600–800 nm is deemed as a good proxy for actual vegetation photosynthesis, showing a close correlation with gross primary productivity (GPP) (Baker, 2008; Li et al., 2018; Porcar-Castell et al., 2014; Sun et al., 2017). With the release of long-term SIF products, it has become feasible to investigate the impacts of recent climate and CO_2 trends on vegetation productivity using satellite SIF data. These satellite-based SIF observations have shown great potential to reveal changes in global vegetation productivity in response to climate change (Guanter et al., 2014; Li et al., 2018; Zhang et al., 2014). Compared to other remotely sensed proxies, the use of satellite-based SIF data provides a novel perspective to understand the relationships between global vegetation productivity and its drivers.

Here, we evaluated the relative impacts of recent climate and CO_2 trends on global vegetation productivity over the last two decades using a robust ensemble of satellite- and flux tower-observed data. We analyzed the trends in VPD, temperature, and atmospheric CO_2 concentration over globally vegetated areas. Meanwhile, we examined the trends in global vegetation productivity using SIF and GPP datasets. Moreover, two types of experimental simulation based on the linear least square regression method were used to estimate the SIF (or GPP) sensitivities to VPD, temperature, and atmospheric CO_2 concentration. On this basis, we calculated the relative contributions of VPD, temperature, and atmospheric CO_2 concentration to SIF (or GPP). We aim to address the following questions: (a) Has global vegetation productivity increased or decreased under recent climate and CO_2 trends? (b) What are the relative impacts of VPD, temperature, and atmospheric CO_2 concentration on global vegetation productivity? (c) To what extent did rising VPD reduce global vegetation productivity?

2. Materials and Methods

2.1. Data

2.1.1. Global Land Cover Data

The Moderate Resolution Imaging Spectroradiometer (MODIS) land cover type data set (MCD12C1) with the classification scheme of the International Geosphere-Biosphere Program was used to determine global vegetation cover for 2001–2019 with a spatial resolution of 0.05°. To minimize the effect of land cover change,

the transformations between the vegetated and non-vegetated areas were not considered in this study. We overlay the vegetation layers of 2001–2019 to ensure that each studied grid cell was a multi-year vegetated zone.

2.1.2. Climate and CO_2 Data

The monthly global gridded VPD, temperature, precipitation, and downward shortwave radiation data were obtained from TerraClimate (Abatzoglou et al., 2018), a high-spatial-resolution climate dataset (1/24°, i.e., approximately 0.0417°). It combines climate variables from the WorldClim, Japanese 55-year Reanalysis (JRA-55), and Climate Research Unit datasets using the climatologically aided interpolation approach. The monthly global gridded atmospheric CO_2 concentration data were obtained from the CarbonTracker dataset (CT2019B), providing estimates of surface-atmosphere CO_2 fluxes on the global $3° \times 2°$ grid from 2000 to 2018 (Jacobson et al., 2020). In addition, we also used the annual in situ CO_2 measurements at Barrow, Mauna Loa, American Samoa, and South Pole to compare with the gridded CO_2 data.

2.1.3. Satellite-Based SIF and GPP Products

We used two satellite-based SIF datasets derived from the Orbiting Carbon Observatory-2 (OCO-2) SIF observations as proxies for vegetation photosynthesis, that is, a global "OCO-2" SIF product (GOSIF; Li & Xiao, 2019) and a global spatially contiguous SIF product (CSIF; Zhang et al., 2018). The GOSIF product was produced by a combination of discrete OCO-2 SIF soundings, MODIS data, and meteorological reanalysis data using a data-driven approach (Li & Xiao, 2019). The GOSIF data from 2000 to 2018 were used as the primary SIF dataset to conduct this study. The CSIF product was produced by training a neural network with the OCO-2 SIF and MODIS data (Zhang et al., 2018). The CSIF data in all-sky conditions from 2001 to 2016 were used as the secondary SIF dataset to compare with the GOSIF results. Moreover, we used the Vegetation Photosynthesis Model-based GPP (VPM GPP) data from 2000 to 2016 to compare with the SIF results. The VPM GPP dataset is based on an improved light use efficiency theory with a separate treatment for C3 and C4 photosynthesis pathways, showing a good simulation of the vegetation photosynthesis process (Zhang, Xiao, et al., 2017). All the gridded SIF and GPP data are available globally at a spatial resolution of 0.05°.

2.1.4. Flux Tower Data

The flux tower-based climate, CO_2, and GPP data were obtained from the latest global eddy covariance flux dataset, FLUXNET2015 (Pastorello et al., 2020). We used the annual mean GPP estimates based on the night-time partitioning method (i.e., "GPP_NT_VUT_REF") (Reichstein et al., 2005). The flux tower-based data were used to evaluate the robustness of the results from satellite-based datasets. To explore the long-term trends in flux tower-based GPP, we compiled a database consisting of 62 flux tower sites having at least 8 years of valid GPP estimates since 2000 (Figure S1 and Table S1 in Supporting Information S1). Our selection criteria of flux tower sites followed to the previous studies (Chen et al., 2020; Wang et al., 2019).

2.2. Methods

2.2.1. Pre-Processing

For the gridded data, we aggregated all of them into a 0.05° spatial resolution and a monthly temporal resolution. We calculated the annual growing season mean climate variables (i.e., VPD, temperature, precipitation, and downward shortwave radiation), atmospheric CO_2 concentration, SIF, and GPP by averaging their monthly values for months with mean temperatures above 0 °C, excluding non-vegetated areas (He et al., 2021; Yuan et al., 2019). For the flux tower-based data, the number of the months per year with monthly mean temperatures above 0 °C were varying at some sites. It is therefore difficult to define a constant growing season length for each site. As such, we used the annual mean values instead of the annual growing season mean values to conduct the following analysis (Wang et al., 2021).

2.2.2. Trend Analysis

The trends in VPD, temperature, atmospheric CO_2 concentration, SIF, and GPP at global and site scales were estimated using the linear least square regression method with a two-tailed *t*-test. Moreover, we used the Theil-Sen estimator with a Mann-Kendall test to estimate their trends for each grid cell across the globe (Wang et al., 2019; Zhu et al., 2016). Besides, we calculated the normalized anomalies of global mean VPD, temperature, SIF, and GPP to further compare the VPD trend with the temperature trend, and the SIF trends with the GPP trend (Jiao

et al., 2019, 2021). We estimated the trends in their normalized anomalies using the linear least square regression method with a two-tailed *t*-test. The normalized anomalies were calculated using the following equation:

$$\mathrm{var}'_t = \left(\mathrm{var}_t - \overline{\mathrm{var}}\right) / \sigma_{\mathrm{var}}, \tag{1}$$

where var'_t represents the normalized anomaly of the variable at time t; var_t represents the value of the variable at time t; $\overline{\mathrm{var}}$ and σ_{var} represent the mean and standard deviation of the variable over the whole study period, respectively.

2.2.3. Experimental Simulation Design

To isolate the relative impacts of VPD, temperature, and atmospheric CO_2 concentration on SIF (or GPP), we designed two types of simulation experiments using the linear least square regression method based on the following equation (Liu et al., 2019; Yuan et al., 2019):

$$\mathrm{y} = \beta_0 + \beta_1 \times \mathrm{VPD} + \beta_2 \times \mathrm{T} + \beta_3 \times \mathrm{Prec} + \beta_4 \times \mathrm{Srad} + \beta_5 \times \mathrm{CO_2} + \varepsilon, \tag{2}$$

where y is the observed/simulated SIF (or GPP); VPD, T, Prec, Srad, and CO_2 represent the observed values of VPD, temperature, precipitation, downward shortwave radiation, and atmospheric CO_2 concentration, respectively; β_1, β_2, β_3, β_4, and β_5 represent regression coefficients; β_0 is the intercept; ε is the residual. The first type of simulation experiment (S_{ALL}) was a normal model run, and all the variables (i.e., VPD, T, Prec, Srad, and CO_2) were set to change with time. The second type of simulation experiments (S_{VPD0}, S_{T0}, and S_{CO20}) were the simulation experiments conducted by holding VPD, T, and CO_2 constant, respectively. Specifically, we held one of the three variables (i.e., VPD, T, and CO_2) constant at an initial baseline level, while allowing Prec, Srad, and the other two variables to change with time. The initial baseline levels were defined as the values of VPD, T, and CO_2 in the first year of the SIF (or GPP) datasets. For instance, the S_{VPD0} simulation experiment using GOSIF was conducted by holding VPD constant at its 2000 level and varying T, Prec, Srad, and CO_2 from 2000 to 2018. Similarly, the S_{T0} and S_{CO20} simulation experiments using GOSIF were conducted by holding T and CO_2 at their 2000 levels, respectively, and varying the other four variables from 2000 to 2018.

2.2.4. Sensitivity Analysis

We used the differences between the simulation results of the first type (S_{ALL}) and the second type (S_{VPD0}, S_{T0}, and S_{CO20}) to estimate the sensitivities of SIF (or GPP) to VPD (β_{VPD}), temperature (β_{T}), and atmospheric CO_2 concentration (β_{CO2}) (Liu et al., 2019; Yuan et al., 2019). Specifically, β_{VPD}, β_{T}, and β_{CO2} were calculated using the following equations:

$$\Delta \mathrm{y}_{(S_{\mathrm{ALL}} - S_{\mathrm{VPD0}})} = \beta_0 + \beta_{\mathrm{VPD}} \times \Delta \mathrm{VPD}_{(S_{\mathrm{ALL}} - S_{\mathrm{VPD0}})} + \varepsilon, \tag{3}$$

$$\Delta \mathrm{y}_{(S_{\mathrm{ALL}} - S_{\mathrm{T0}})} = \beta_0 + \beta_{\mathrm{T}} \times \Delta \mathrm{T}_{(S_{\mathrm{ALL}} - S_{\mathrm{T0}})} + \varepsilon, \tag{4}$$

$$\Delta \mathrm{y}_{(S_{\mathrm{ALL}} - S_{\mathrm{CO20}})} = \beta_0 + \beta_{\mathrm{CO2}} \times \Delta \mathrm{CO2}_{(S_{\mathrm{ALL}} - S_{\mathrm{CO20}})} + \varepsilon, \tag{5}$$

where $\Delta \mathrm{y}$, $\Delta \mathrm{VPD}_{(S_{\mathrm{ALL}} - S_{\mathrm{VPD0}})}$, $\Delta \mathrm{T}_{(S_{\mathrm{ALL}} - S_{\mathrm{T0}})}$, and $\Delta \mathrm{CO2}_{(S_{\mathrm{ALL}} - S_{\mathrm{CO20}})}$ represent the differences in SIF (or GPP), VPD, temperature, and atmospheric CO_2 concentration between the two types of experimental simulations, respectively; β_0 is the intercept; ε is the residual. We calculated the sensitivities of global SIF (or GPP) to VPD, temperature, and atmospheric CO_2 concentration, as well as the sensitivities of SIF (or GPP) to these three variables for each grid cell and each flux tower site. In addition, we conducted the partial correlation analysis for each grid cell to evaluate whether VPD and temperature had the different impacts on SIF (or GPP) over most of the globally vegetated areas (Yuan et al., 2019). We analyzed partial correlations of detrended SIF (or GPP) with detrended VPD and temperature by excluding the effects of precipitation, downward shortwave radiation, and atmospheric CO_2 concentration.

2.2.5. Contribution Analysis

Based on the estimated SIF (or GPP) sensitivities to VPD, temperature, and atmospheric CO_2 concentration, we calculated their relative contributions to SIF (or GPP) using the following equation (Yuan et al., 2019):

$$Con = \beta_{\mathrm{Trend}} \times \beta_{\mathrm{Sen}}, \tag{6}$$

where *Con* represents the contributions of VPD, temperature, and atmospheric CO_2 concentration to SIF (or GPP); β_{Trend} represents the trends of VPD, temperature, and atmospheric CO_2 concentration; β_{Sen} represents the sensitivities of SIF (or GPP) to VPD, temperature, and atmospheric CO_2 concentration. We calculated the contributions of VPD, temperature, and atmospheric CO_2 concentration to global SIF (or GPP), as well as the contributions of these three variables to SIF (or GPP) for each grid cell and each flux tower site.

The percentages of the SIF (or GPP) decrease due to the increased VPD (VPD_{Inc}) in the warming and CO_2-induced SIF (or GPP) increases were determined using the following equations (Fernandez-Martinez et al., 2019; Wang et al., 2019):

$$\%\mathrm{VPD_W} = \frac{|Con.\mathrm{VPD_{Inc}}|}{Con.\mathrm{W}} \times 100\%, \tag{7}$$

$$\%\mathrm{VPD_{CO2}} = \frac{|Con.\mathrm{VPD_{Inc}}|}{Con.\mathrm{CO2}} \times 100\%, \tag{8}$$

$$\%\mathrm{VPD_{W+CO2}} = \frac{|Con.\mathrm{VPD_{Inc}}|}{Con.\mathrm{W} + Con.\mathrm{CO2}} \times 100\%, \tag{9}$$

where $\%VPD_W$, $\%VPD_{CO2}$, and $\%VPD_{W+CO2}$ represent the percentages of the negative contribution of the increased VPD in the positive contributions of warming, CO_2, and both together (i.e., warming+CO_2), respectively; *Con.*VPD_{Inc} represents the negative contribution of VPD_{Inc} to SIF (or GPP), that is, the VPD_{Inc}-induced decrease; *Con.*W represents the positive contribution of warming to SIF (or GPP), that is, the warming-induced increase; *Con.*CO2 represents the positive contribution of elevated CO_2 concentration to SIF (or GPP), that is, the CO_2-induced increase.

It is worth noting that the standard errors of *Con*, $\%VPD_W$, $\%VPD_{CO2}$, and $\%VPD_{W+CO2}$ in Equations 6–9 were propagated from the standard errors of their related variables. The propagated standard errors were calculated using the error-propagation method with the following equations (Fernandez-Martinez et al., 2019):

$$\sigma_x^2 = \sigma_u^2 + \sigma_v^2 + \cdots + \sigma_n^2, \tag{10}$$

$$\frac{\sigma_x^2}{x^2} = \frac{\sigma_u^2}{u^2} + \frac{\sigma_v^2}{v^2} + \cdots + \frac{\sigma_n^2}{n^2}, \tag{11}$$

where σ_x represents the propagated standard errors, σ_u, σ_v, and σ_n represent the standard errors, and x, u, and v represent the estimated values. We used Equation 10 to estimate the propagated standard errors for addition and subtraction, and Equation 11 to estimate the propagated standard errors for multiplication and division.

3. Results

3.1. Trends in VPD, Temperature, and Atmospheric CO_2 Concentration

Here, we analyzed the trends in the annual growing season mean VPD, temperature, and atmospheric CO_2 concentration over the globally vegetated areas during recent decades. Our results indicated that there was an overall rise in VPD, temperature, and atmospheric CO_2 concentration. Specifically, we found that both VPD and temperature rose in steps (two-tailed *t*-test: $P < 0.05$), showing higher levels in 2000–2019 than in 1960–1979 and 1980–1999 (Figure 1a). VPD anomalies increased more rapidly during 2000–2019 (slope = 0.16 ± 0.02) than during the two earlier periods (slope = 0.02 ± 0.01 and 0.01 ± 0.01, respectively). Moreover, we also examined the spatial patterns of the trends in VPD and temperature during 2000–2019 over vegetated areas. It was observed that 75.63% of vegetated grid cells had an increase in VPD (23.36% with a significant increase, Mann-Kendall test: $P < 0.05$) (Figure 1b), and 79.49% of vegetated grid cells had an increase in temperature (23.45% with a significant increase, Mann-Kendall test: $P < 0.05$) (Figure 1c). In addition, global atmospheric CO_2 concentration maintained a significantly rising trend (two-tailed *t*-test: $P < 0.05$) (Figure S2a in Supporting Information S1), and all the vegetated areas experienced a significant increase in atmospheric CO_2 concentration during 2000–2018 (Mann-Kendall test: $P < 0.05$) (Figure S2b in Supporting Information S1).

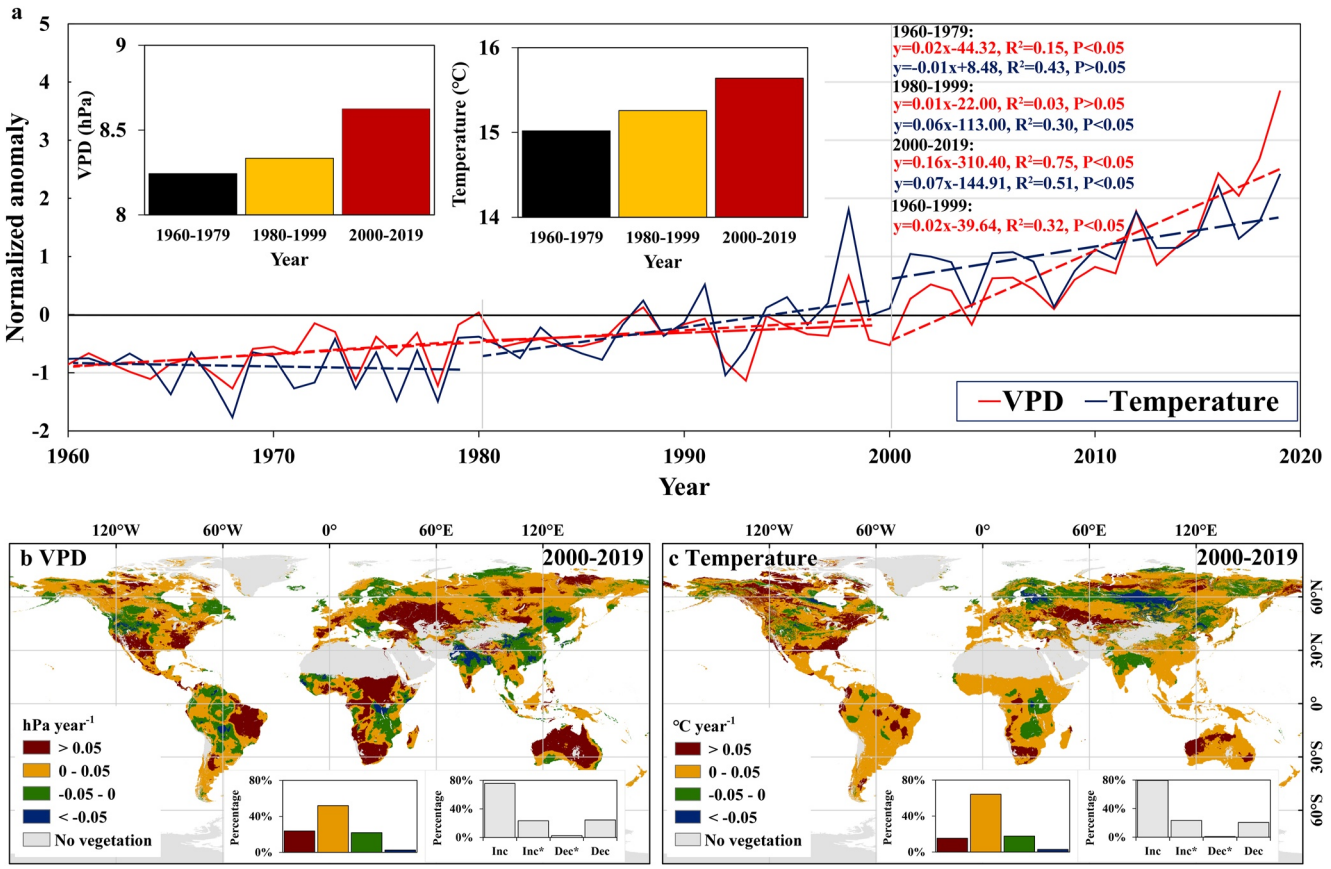

Figure 1. Trends in vapor pressure deficit (VPD) and temperature over the last decades. (a) Time series of normalized anomalies of the annual growing season mean VPD and temperature over the globally vegetated areas during 1960–2019. (b) Spatial pattern of the trends in the annual growing season mean VPD over vegetated areas during 2000–2019. (c) Spatial pattern of the trends in the annual growing season mean temperature over vegetated areas during 2000–2019. The mean values of VPD and temperature during 1960–2019 are 8.4 hPa and 15.3°C, respectively, and the standard deviations are 0.2 hPa and 0.3°C, respectively. The insets in (a) show the annual growing season mean VPD and temperature over vegetated areas during the three periods. The left insets in (b) and (c) show the frequency distributions of the corresponding ranges, and the right insets show the relative frequency distributions of increases (Inc), significant increases (Inc*; Mann-Kendall test: $P < 0.05$), significant decreases (Dec*; Mann-Kendall test: $P < 0.05$), and decreases (Dec).

3.2. Satellite- and Flux Tower-Observed Trends in Global Vegetation Productivity

Although rising VPD can limit vegetation growth to some extent, multiple lines of evidence showed that global vegetation productivity has increased during the last two decades. Specifically, we found that SIF (or GPP) anomalies significantly increased over the growing season (two-tailed *t*-test: $P < 0.05$) (Figure 2a). Global GOSIF increased at a rate of 0.0055 ± 0.0005 W m^{-2} μm^{-1} sr^{-1} decade^{-1} during 2000–2018. Global CSIF and VPM GPP increased at rates of 0.0035 ± 0.0007 W m^{-2} μm^{-1} sr^{-1} decade^{-1} and 0.1745 ± 0.0167 gC m^{-2} d^{-1} decade^{-1} during 2001–2016 and 2000–2016, respectively. Moreover, we examined the spatial patterns of the trends in the annual growing season SIF (or GPP) over the globally vegetated areas (Figures 2b–2d). According to the GOSIF results, 72.2% of vegetated grid cells had an increase in SIF (23.7% with a significant increase, Mann-Kendall test: $P < 0.05$) (Figure 2b). Similarly, the CSIF and VPM GPP results showed that 66.5% and 74.6% of vegetated grid cells had an increase in SIF and GPP, respectively (14.0% and 26.8% with a significant increase, Mann-Kendall test: $P < 0.05$) (Figures 2c and 2d). In addition, we analyzed the trends in flux tower-based GPP at 62 sites to evaluate the robustness of the results from satellite-based datasets. We found that more than 50% of the sites had an increase in GPP (34 sites, 15 sites with a significant increase, two-tailed *t*-test: $P < 0.05$) and only five sites with a significant decrease in GPP (two-tailed *t*-test: $P < 0.05$) (Figure 2e and Table S1 in Supporting Information S1).

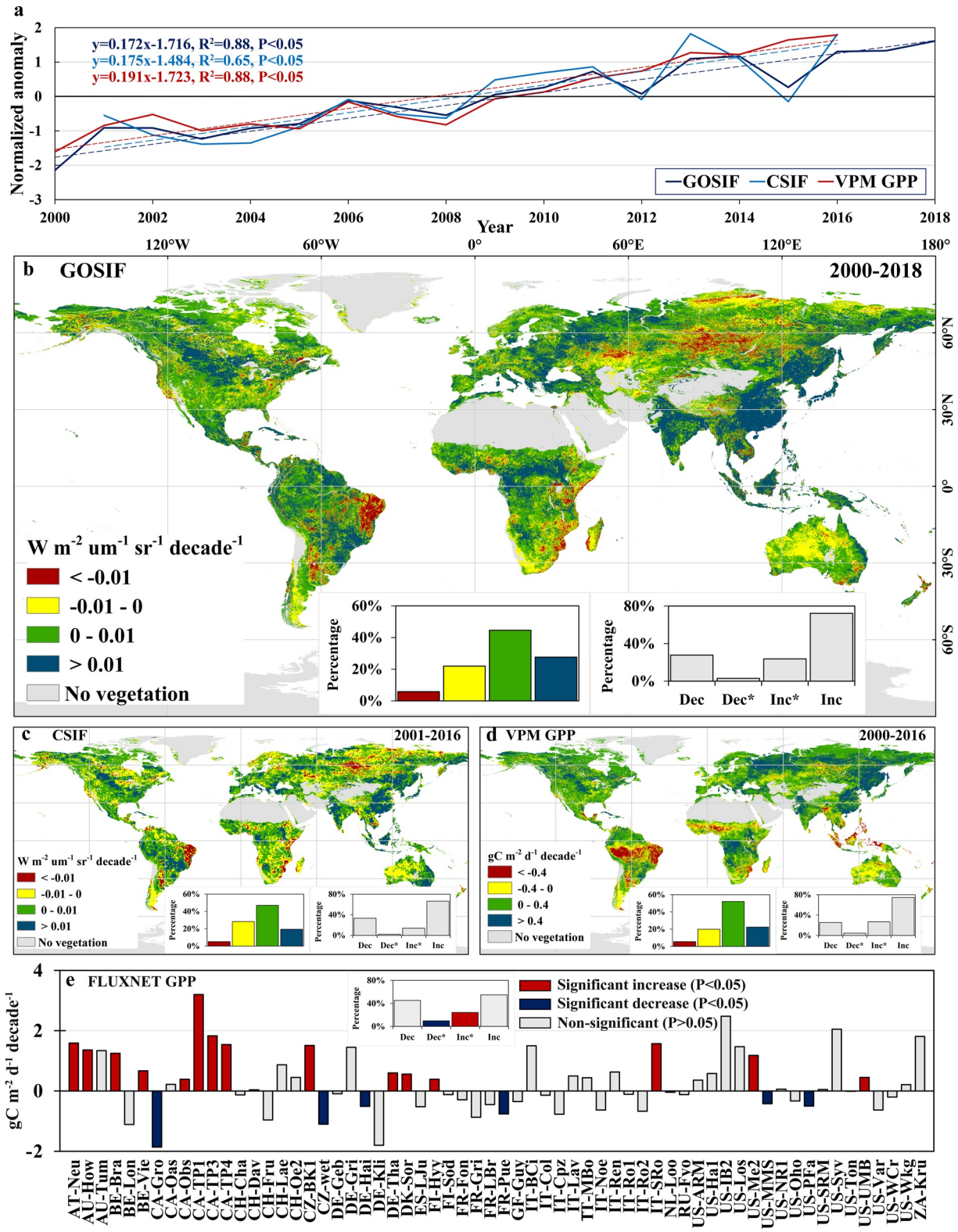
a
y=0.172x-1.716, R²=0.88, P<0.05
y=0.175x-1.484, R²=0.65, P<0.05
y=0.191x-1.723, R²=0.88, P<0.05
Normalized anomaly
GOSIF CSIF VPM GPP
Year
b GOSIF 2000-2018
W m-2 um-1 sr-1 decade-1
< -0.01
-0.01 - 0
0 - 0.01
> 0.01
No vegetation
Percentage
Dec Dec* Inc* Inc
c CSIF 2001-2016
d VPM GPP 2000-2016
gC m-2 d-1 decade-1
< -0.4
-0.4 - 0
0 - 0.4
> 0.4
e FLUXNET GPP
Significant increase (P<0.05)
Significant decrease (P<0.05)
Non-significant (P>0.05)
gC m-2 d-1 decade-1
AT-Neu AU-How AU-Tum BE-Bra BE-Lon BE-Vie CA-Gro CA-Oas CA-Obs CA-TP1 CA-TP3 CA-TP4 CH-Cha CH-Dav CH-Fru CH-Lae CH-Oe2 CZ-BK1 CZ-wet DE-Geb DE-Gri DE-Hai DE-Kli DE-Tha DK-Sor ES-LJu FI-Hyy FI-Sod FR-Fon FR-Gri FR-LBr FR-Pue GF-Guy IT-BCi IT-Col IT-Cpz IT-Lav IT-MBo IT-Noe IT-Ren IT-Ro1 IT-Ro2 IT-SRo NL-Loo RU-Fyo US-ARM US-Ha1 US-IB2 US-Los US-Me2 US-MMS US-NR1 US-Oho US-PFa US-SRM US-Syv US-Ton US-UMB US-Var US-WCr US-Wkg ZA-Kru

Figure 2.

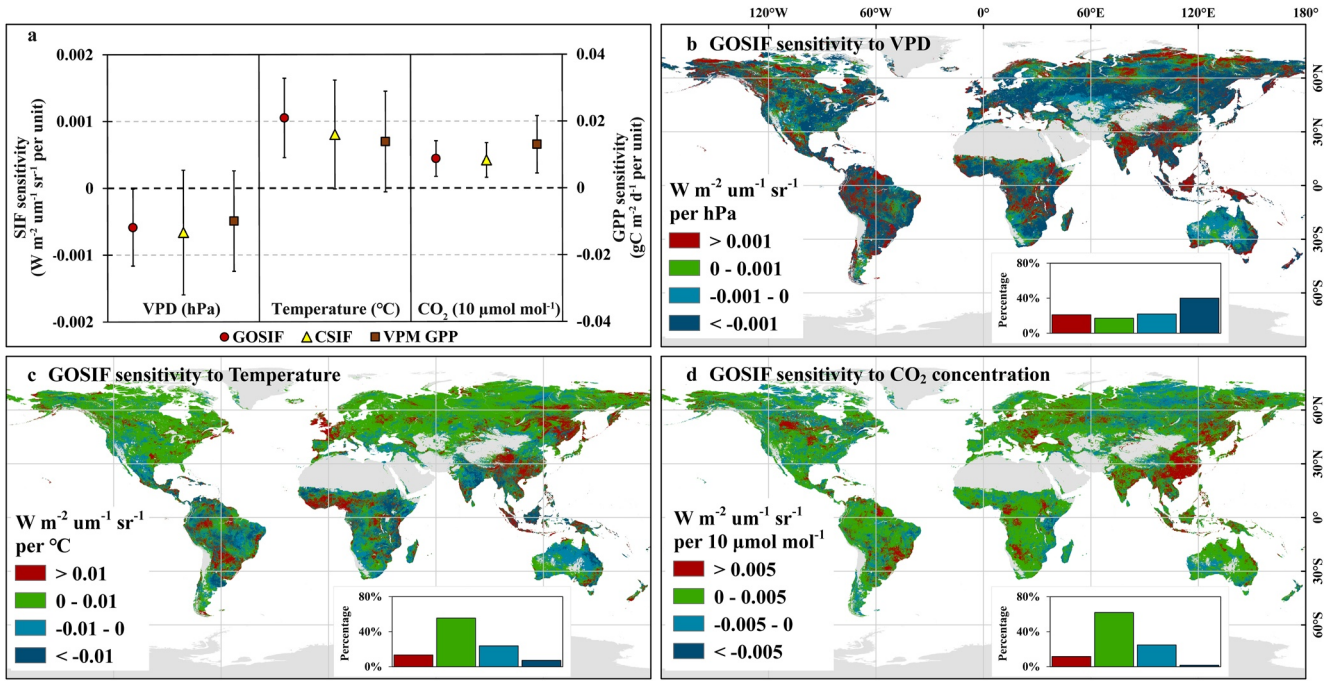

Figure 3. Sensitivities of global vegetation productivity to vapor pressure deficit (VPD), temperature, and atmospheric carbon dioxide (CO_2) concentration. (a) Sensitivities of global solar-induced chlorophyll fluorescence (SIF) (or gross primary productivity (GPP)) to VPD, temperature, and atmospheric CO_2 concentration. (b–d) Spatial patterns of the global "OCO-2" SIF product (GOSIF) sensitivities to VPD, temperature, and atmospheric CO_2 concentration. The error bars in (a) indicate the standard errors. The insets in (b–d) show the frequency distributions of the corresponding ranges.

3.3. Relative Impacts of VPD, Temperature, and Atmospheric CO_2 Concentration

To estimate the SIF (or GPP) sensitivities to VPD, temperature, and atmospheric CO_2 concentration, we performed two types of experimental simulations based on the linear least square regression method. Our results showed that the sensitivities of global SIF (or GPP) to VPD were negative, and those to temperature and CO_2 concentration were positive (Figure 3a and Table S3 in Supporting Information S1). Moreover, we evaluated the spatial patterns of the SIF (or GPP) sensitivities to these variables for each grid cell using the same method. Our results showed the similar spatial patterns of the SIF (or GPP) sensitivities to VPD, temperature, and atmospheric CO_2 concentration across the globe (Figures 3b–3d and Figure S3 in Supporting Information S1). For instance, the GOSIF results showed that the estimated SIF sensitivity to VPD was negative over 61.9% of vegetated grid cells (Figure 3b). However, the estimated SIF sensitivity to temperature was positive over 68.9% of vegetated grid cells, which was mainly distributed in the Northern Hemisphere, especially at high latitudes (Figure 3c). Meanwhile, the estimated SIF sensitivity to atmospheric CO_2 concentration was positive over 73.5% of vegetated grid cells (Figure 3d). In addition, partial correlation analysis showed that the correlations of SIF (or GPP) with VPD were negative but those with temperature were positive over most of vegetated grid cells (Figure S4 in Supporting Information S1), implying that VPD and temperature had the different impacts on SIF (or GPP).

Based on the estimated SIF (or GPP) sensitivities, we examined the relative contributions of VPD, temperature, and atmospheric CO_2 concentration to global SIF (or GPP) (Figure 4a and Table S4 in Supporting Information S1). For global SIF (or GPP), the decrease due to rising VPD was comparable to the increase due to warming

Figure 2. Increased global vegetation productivity over the last two decades. (a) Time series of normalized anomalies of the annual growing season mean global "OCO-2" SIF product (GOSIF), contiguous SIF product (CSIF), and VPM GPP over the globally vegetated areas. (b) Spatial pattern of the trends in the annual growing season mean GOSIF over vegetated areas during 2000–2018. (c) Spatial pattern of the trends in the annual growing season mean CSIF over vegetated areas during 2001–2016. (d) Spatial pattern of the trends in the annual growing season mean VPM GPP over vegetated areas during 2000–2016. (e) Trends of annual mean GPP at 62 FLUXNET sites. The mean values of GOSIF, CSIF, and VPM GPP are 0.1429 W m^{-2} μm^{-1} sr^{-1}, 0.1211 W m^{-2} μm^{-1} sr^{-1}, and 3.3567 gC m^{-2} d^{-1}, respectively, and the standard deviations are 0.0032 W m^{-2} μm^{-1} sr^{-1}, 0.0020 W m^{-2} μm^{-1} sr^{-1}, and 0.0912 gC m^{-2} d^{-1}, respectively. The left insets in (b–d) show the frequency distributions of the corresponding ranges, and the right insets show the relative frequency distributions of decreases (Dec), significant decreases (Dec*; Mann-Kendall test: $P < 0.05$), significant increases (Inc*; Mann-Kendall test: $P < 0.05$), and increases (Inc). The inset in (e) shows the relative frequency distributions of decreases (Dec), significant decreases (Dec*; two-tailed *t*-test: $P < 0.05$), significant increases (Inc*; two-tailed *t*-test: $P < 0.05$), and increases (Inc).

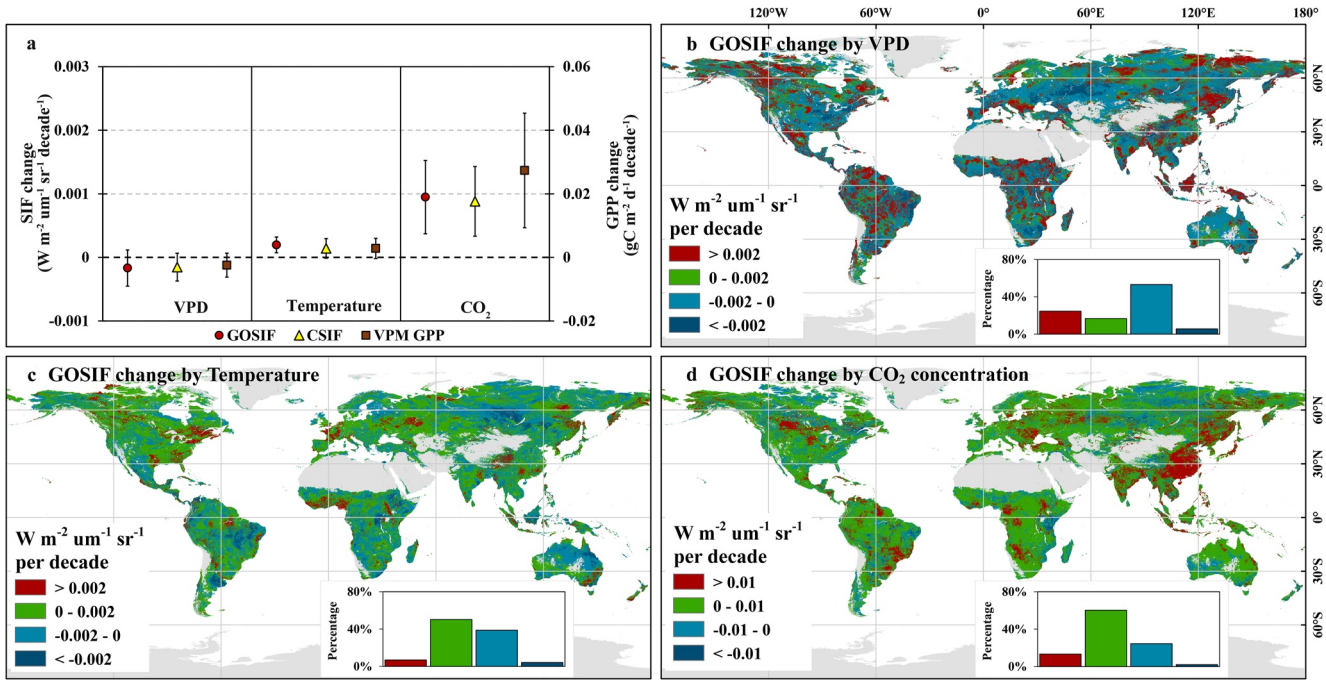

Figure 4. Relative contributions of vapor pressure deficit (VPD), temperature, and atmospheric carbon dioxide (CO_2) concentration to global vegetation productivity. (a) Relative contributions of VPD, temperature, and atmospheric CO_2 concentration to global solar-induced chlorophyll fluorescence (SIF) (or gross primary productivity (GPP)). (b–d) Spatial patterns of the relative contributions of VPD, temperature, and atmospheric CO_2 concentration to global "OCO-2" SIF product (GOSIF). The error bars in (a) indicate the propagated standard errors. The insets in (b–d) show the frequency distributions of the corresponding changes.

but far less than the increase due to elevated CO_2 concentration. Specifically, the VPD_{Inc} led to declines in global GOSIF, CSIF, and VPM GPP, contributing to approximately −3.6%, −5.7%, and −1.4% of each growth, respectively. The increased temperature led to increases in global GOSIF, CSIF, and VPM GPP, contributing to approximately 3.6%, 2.9%, and 1.6% of each growth, respectively. The elevated CO_2 concentration led to increases in global GOSIF, CSIF, and VPM GPP, contributing to approximately 16.4%, 25.7%, and 15.7% of each growth, respectively. Moreover, we evaluated the spatial patterns of the relative contributions of VPD, temperature, and atmospheric CO_2 concentration to SIF (or GPP) for each grid cell using the same method (Figures 4b–4d and Figure S5 in Supporting Information S1). For instance, the GOSIF results showed that VPD led to a SIF decrease over 58.8% of vegetated grid cells (Figure 4b), temperature led to a SIF increase over 57.1% of vegetated grid cells (Figure 4c), and atmospheric CO_2 concentration led to a SIF increase over 72.2% of vegetated grid cells (Figure 4d).

To further evaluate the robustness of the results from satellite-based datasets, we estimated the GPP sensitivities to VPD, temperature, and atmospheric CO_2 concentration at the flux tower sites with a significant trend in GPP. The results showed that GPP had a negative sensitivity to VPD and positive sensitivities to temperature and CO_2 concentration at most sites of cold or dry areas (Figure S6a and Table S5 in Supporting Information S1). We then examined the relative contributions of VPD, temperature, and atmospheric CO_2 concentration to GPP (Figure S6b and Table S6 in Supporting Information S1). The results showed that the contributions of atmospheric CO_2 concentration to GPP were positive and large at most sites, excluding the sites with a significant decrease in GPP. However, the contributions of VPD and temperature to GPP were not comparable to the satellite-based results, since the trends in annual mean VPD and temperature were non-significant (two-tailed *t*-test: $P > 0.05$).

3.4. Roles of Rising VPD in Counteracting the Warming and CO_2 Fertilization Effects

Our above findings have demonstrated the relative impacts of VPD, temperature, and atmospheric CO_2 concentration on global vegetation productivity over the last two decades, yet it seems that global vegetation productivity did not decrease so much due to rising VPD. We found that the VPD_{Inc}-induced decrease counteracted 14.7% ± 26.0%, 15.0% ± 22.9%, and 8.1% ± 13.4% of the warming + CO_2-induced increase of GOSIF, CSIF, and

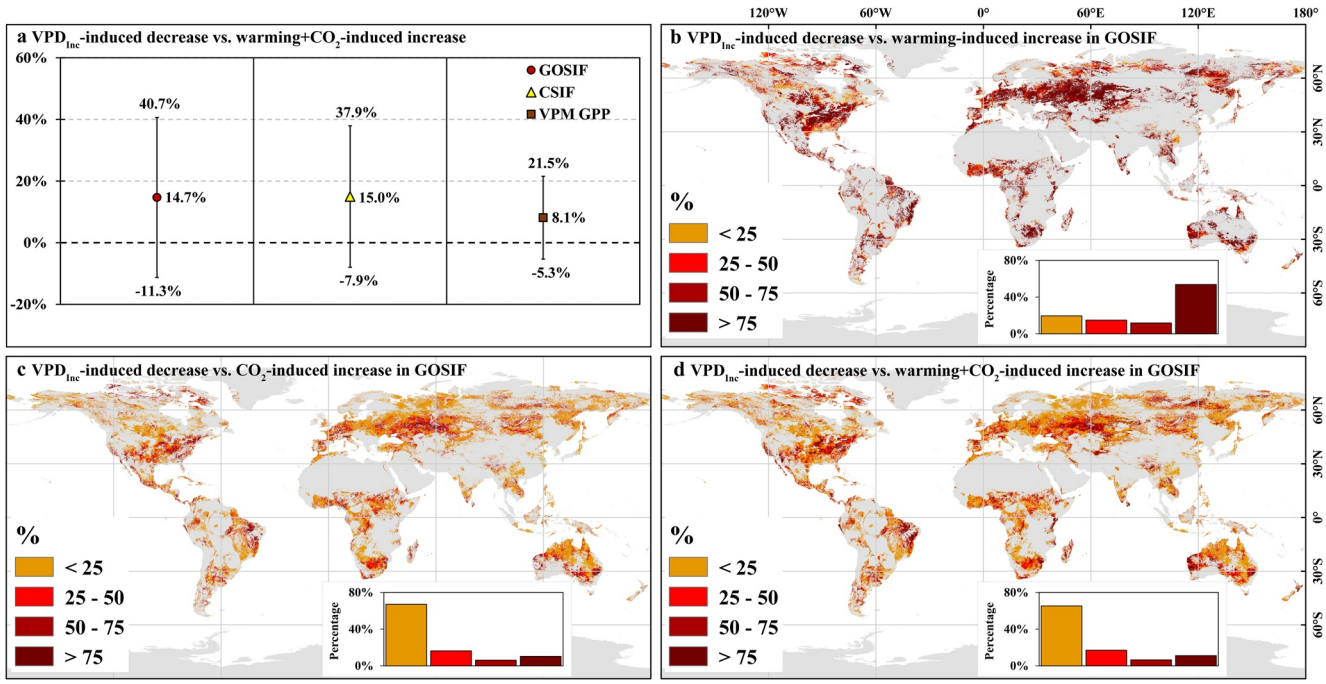

Figure 5. Comparisons of the VPD$_{Inc}$-induced decrease with the warming and CO$_2$-induced increases in global vegetation productivity. (a) Percentages of the VPD$_{Inc}$-induced global solar-induced chlorophyll fluorescence (SIF) (or gross primary productivity (GPP) decrease in the warming+CO$_2$-induced global SIF (or GPP) increase. (b) Spatial pattern of the percentages of the VPD$_{Inc}$-induced global "OCO-2" SIF product (GOSIF) decrease in the warming-induced GOSIF increase. (c) Spatial pattern of the percentages of the VPD$_{Inc}$-induced GOSIF decrease in the CO$_2$-induced GOSIF increase. (d) Spatial pattern of the percentages of the VPD$_{Inc}$-induced GOSIF decrease in the warming+CO$_2$-induced GOSIF increase. The error bars in (a) indicate the propagated standard errors. The insets in (b–d) show the frequency distributions of the corresponding ranges.

VPM GPP, respectively (Figure 5a). Considering the strong positive impacts of the warming and CO$_2$ fertilization effects on vegetation, rising VPD did not actually result in a large net loss in SIF or GPP. Moreover, we separated the VPD$_{Inc}$-induced decrease, the warming-induced increase, and the CO$_2$-induced increase in SIF (or GPP) for each grid cell (Figure S7 in Supporting Information S1). On this basis, we examined the spatial patterns of the percentages of the VPD$_{Inc}$-induced SIF (or GPP) decrease relative to the warming-induced SIF (or GPP) increase, the CO$_2$-induced SIF (or GPP) increase, and the warming + CO$_2$-induced SIF (or GPP) increase (Figures 5b–5d and Figure S8 in Supporting Information S1). As expected, the spatial patterns also showed that the actual negative impacts of rising VPD on vegetation productivity were much smaller than the benefit from the warming and CO$_2$ fertilization effects in most areas.

4. Discussion

It is critical to evaluate trends in global vegetation productivity for understanding the terrestrial carbon cycle, especially in the context of climate change (Falkowski et al., 2000; Piao et al., 2013; Xiao et al., 2019). In this study, we conducted a comprehensive evaluation of trends in global vegetation productivity using a robust ensemble of SIF and GPP data. Multiple lines of evidence indicated that global vegetation productivity has increased over the last two decades (Figure 2). Similar to the previous results based on VIs (Myneni et al., 1997; Zhang, Song, et al., 2017; Zhu et al., 2016), our results showed that SIF (or GPP) has increased over more than half (approximately 66.5%–72.2%) of the globally vegetated areas. Most of the upward trends were found in East Asia, South Asia, Central Africa, central North America, and continental Europe. We found that the spatial patterns of the SIF (or GPP) trend were consistent with those of greening trends (Zhang, Song, et al., 2017; Zhu et al., 2016). Moreover, we found a remarkable difference between the SIF and GPP trends in the southern Amazon, that is, a decrease in GPP but an increase in SIF. Unlike those decreases due to extensive deforestation in eastern Brazil (De Sy et al., 2015; Malhi et al., 2008), the GPP decline in the southern Amazon could be attributed to drought events (Doughty et al., 2015; Saatchi et al., 2013). However, a recent study reported that the negative impacts of increases in atmospheric and soil dryness on Amazonian rainforest productivity were overestimated (Green

et al., 2020). In our study, we also found that rising VPD had a small negative impact or even a positive impact on SIF in the Amazon area. Due to the lack of field observations, it would be challenging to determine which of the SIF-based or GPP-based results capture the actual trend in the rainforest vegetation productivity.

It has been widely reported that rising VPD can reduce global vegetation productivity (Konings & Gentine, 2017; Lopez et al., 2021; Yuan et al., 2019). In this study, we examined the recent trends in VPD, temperature, and atmospheric CO_2 concentration and their relative impacts on global vegetation productivity. Our results showed that global VPD has increased more rapidly than temperature and CO_2 concentration during the last two decades (Figure 1a and Figure S2a in Supporting Information S1). Previous studies indicated that the sharp increase in global VPD is attributed to both the increase in saturated vapor pressure and the decrease in actual vapor pressure (Ficklin & Novick, 2017; Willett et al., 2014; Yuan et al., 2019). Increased VPD is expected to limit vegetation photosynthesis at the leaf scale by decreasing stomatal conductance and increasing nonphotochemical quenching (Flexas et al., 2002; Lu et al., 2018; Shan et al., 2021). In our study, we found that VPD has a negative impact on SIF (or GPP) over more than 50% of the globally vegetated areas (Figure 3b; Figure S3a and S3b in Supporting Information S1). This is similar to the result reported in a wide-disseminated study (Yuan et al., 2019), that is, VPD has a negative correlation with VIs and LAI over more than 62% of the globally vegetated areas. However, we found that rising VPD counteracted only a small proportion (approximately 8.1%–15.0%) of the warming and CO_2-induced increase (Figure 5a). Previous studies suggested that a much strong impact of rising VPD on GPP counteracted more than half of the CO_2 fertilization effect (He et al., 2021; Yuan et al., 2019). Considering our methods are similar to theirs, the difference could be associated with the different proxies for vegetation productivity. In our study, we used the satellite-based SIF and VPM GPP data to evaluate the relative impact of rising VPD on global vegetation productivity. Compared to their revised eddy covariance-light use efficiency (EC-LUE) and MODIS-based models (Yuan et al., 2019), our results represent changes in global vegetation productivity from satellite SIF observations. The results based on VIs, EC-LUE GPP, and MODIS GPP data indicated that global vegetation productivity has decreased since the year of 1999, but they were non-significant at a global scale and over most of vegetated areas (Yuan et al., 2019). As such, the impact of rising VPD could be overestimated due to the underestimated trends in global vegetation productivity, probably leading to some uncertainties in previous studies.

Unlike the results of field experiments, the satellite-based results at large scales showed that vegetation productivity responses to high VPD could be complicated. A recent study reported that in most of the wettest areas, such as Amazon rainforest, vegetation productivity could increase with rising VPD (Green et al., 2020). Similarly, we also found that VPD_{Inc} has weakly negative or even positive impacts on vegetation productivity in some wet regions, for example, most of southern China, India, and tropical rainforests (Figure 3b; Figure S3a and S3b in Supporting Information S1). It has been reported that high VPD could enhance photosynthetic capacity by accelerating the replacement of old leaves (Green et al., 2020). Moreover, although our findings indicated that the correlations of SIF (or GPP) with VPD are negative and those with temperature are positive in most of vegetated areas (Figures 3b and 3c; Figure S3a–S3d in Supporting Information S1), high VPD often occurs along with high temperature and thus can promote vegetation productivity in cold regions (Liu et al., 2018; Piao et al., 2007, 2019; Xia et al., 2014). Furthermore, the effects of VPD on assimilation and transpiration could be non-linear at the leaf scale. Previous studies reported that stomatal acclimation to high VPD could decrease the stomatal sensitivity to VPD and thus enhance photosynthetic capacity (Grossiord et al., 2020; Lopez et al., 2021). However, it is difficult to discover the non-linear relationships between global vegetation productivity and its drivers at an annual time scale (Wang et al., 2020; Yuan et al., 2019; Zhu et al., 2016). In addition, considering the warming hiatus (Wang et al., 2019) and the declining CO_2 fertilization effects (Penuelas et al., 2017; Wang et al., 2020; Winkler et al., 2021), global vegetation productivity would receive fewer benefits and thus the negative impact of rising VPD would be stronger in the future. Therefore, more studies are needed to further evaluate the roles of VPD on vegetation productivity across different space and time scales.

In this study, we used precipitation data instead of soil moisture data to represent the effects of water availability on vegetation productivity. Analogous to the revised EC-LUE model (Yuan et al., 2010, 2019), our experimental simulations of SIF and GPP were driven by VPD, temperature, precipitation, downward shortwave radiation, and atmospheric CO_2 concentration. Although precipitation is highly correlated with soil moisture over most of the globally vegetated areas, compared with direct soil moisture measurements, precipitation may introduce some bias into our results, especially in some areas with high evapotranspiration (Meng et al., 2018; Nandintsetseg &

Shinoda, 2014). Moreover, the relative role of soil moisture and VPD in reducing global vegetation productivity is under debate in the literature (Fu et al., 2022; Liu et al., 2020). It is challenging to disentangle the relative impacts of soil moisture and VPD on global vegetation productivity. A previous study using satellite SIF observations reported that soil moisture is the dominant driver of dryness stress on ecosystem productivity across more than 70% of the globally vegetated areas (Liu et al., 2020). However, a recent study using flux tower observations found that the decreased GPP was not universally associated with a decrease in soil moisture but was dominated by rising VPD (Fu et al., 2022). These different results could be associated with the different approaches and data used to estimate the relative impacts of soil moisture and VPD. Furthermore, we focus on quantifying the relative impacts of recent climate (i.e., VPD and temperature) and CO_2 trends on global vegetation productivity. Our methods will not allow us to disentangle the roles of variability and trends in soil moisture on vegetation productivity, but based on previous studies (Ahlstrom et al., 2015; Chen et al., 2014; Wang et al., 2014), we expect the impacts of soil moisture variability would be larger than those of its trends on global vegetation productivity. In addition, heat waves and droughts can significantly reduce vegetation productivity at a regional scale. Previous studies indicated that global vegetation productivity could be more vulnerable to heat wave and drought events, especially in drylands (Allen et al., 2015; Breshears et al., 2021). Vegetation water deficit areas were significantly expanding but vegetation water surplus areas were significantly shrinking, suggesting a stronger sensitivity of vegetation to drought (Jiao et al., 2021). Therefore, extreme events such as heat waves and droughts could intensify the impact of VPD and thus cause more decreases in global vegetation productivity.

To isolate the relative impacts of VPD, temperature, and atmospheric CO_2 concentration on SIF (or GPP), we designed two types of simulation experiments. Our results showed that the recent trends in VPD, temperature, and atmospheric CO_2 concentration can explain about 30% of changes in global SIF (or GPP). The effects of nitrogen deposition and land use change on global vegetation productivity were not considered in our study, which may account for 9% and 4% of the positive contributions, respectively (Zhu et al., 2016). We also did not consider the effects of irrigation and fertilization on croplands in our analysis due to a lack of data at a global scale (Fu et al., 2022; Liu et al., 2020; Piao et al., 2015; Yuan et al., 2019). Although human land-use management could lead to an increase in vegetation productivity (Chen et al., 2019), we found that most of the regions with increased vegetation productivity due to agricultural intensification have not experienced an increase in VPD over the last two decades. Moreover, the data we used in this study could also result in a number of uncertainties. Despite previous studies reported that satellite-based SIF is reliable for capturing changes in vegetation productivity (Baker, 2008; Frankenberg et al., 2011; Gu et al., 2019; Guanter et al., 2014; Li et al., 2018; Porcar-Castell et al., 2014; van der Tol et al., 2014), the SIF data derived from the GOSIF and CSIF products are reconstructed estimates but not direct retrievals. The model-based GPP data derived from the VPM GPP and FLUXNET datasets are not direct measurements either. The eddy covariance flux tower sites used in our analysis are mostly distributed in Europe and North America, and the time series of flux tower-based GPP are shorter than those of SIF (or GPP) from satellite-based datasets. The temporal and spatial mismatches between flux tower-based GPP and satellite-based SIF (or GPP) could be another limitation. Furthermore, we did not use process-based global terrestrial biosphere models to conduct additional analyses to compare with our results. Although the use of terrestrial biosphere models would be helpful for improving the robustness of our results (Wang et al., 2020; Winkler et al., 2021), their attribution approaches and coarse resolution outputs could introduce some uncertainties when comparing with the current results (Ding et al., 2020; Ryu et al., 2019; Smith et al., 2016). These models rely on a set of key assumptions and therefore have the limitations on predicting vegetation changes in response to rising CO_2 (De Kauwe et al., 2014; Medlyn et al., 2016; Rifai et al., 2022). Considering that this study aims to show our findings from a perspective of satellite SIF, we think a more fruitful future direction would be improving the spatial resolution of the results to avoid or eliminate the bias due to data quality, instead of comparing the results of additional methods. However, clearly more future work is still needed to further evaluate our findings and minimize uncertainties.

In summary, this study used a robust ensemble of SIF and GPP data to quantify the relative impacts of VPD, temperature, and atmospheric CO_2 concentration on global vegetation productivity over the last two decades. The satellite- and flux tower-based results indicated that there was a significant increase in global vegetation productivity with rising VPD, temperature, and atmospheric CO_2 concentration. Our findings indicated that rising VPD counteracted only a small proportion of the warming and CO_2-induced increase in global SIF (or GPP). While some uncertainties remain in our results, we provide a novel perspective to understand the quantitative contribution of rising atmospheric dryness on global vegetation productivity under concurrent climate warming and CO_2

increasing. More field and experimental studies are still needed to further improve our understanding of climate change impacts on global terrestrial ecosystems.

Conflict of Interest

The authors declare no conflicts of interest relevant to this study.

Data Availability Statement

The monthly global high-resolution gridded climate dataset, TerraClimate, is available at https://www.climatologylab.org/terraclimate.html. The monthly global gridded atmospheric CO_2 concentration data were obtained from the CarbonTracker dataset (CT2019B) at https://gml.noaa.gov/aftp/products/carbontracker/co2/molefractions/co2_total_monthly. The annual in situ CO_2 measurements at Barrow, Mauna Loa, American Samoa, and South Pole were obtained from https://gml.noaa.gov/aftp/data/trace_gases/co2/in-situ/surface/. The MODIS land cover type dataset (MCD12C1) is available at https://lpdaac.usgs.gov/products/mcd12c1v006. The GOSIF dataset was obtained from https://globalecology.unh.edu/data/GOSIF.html. The CSIF dataset was obtained from https://figshare.com/articles/dataset/CSIF/6387494. The VPM GPP dataset was obtained from https://figshare.com/articles/dataset/Monthly_GPP_at_0_05_degree/5048113. The flux tower-based GPP dataset, FLUXNET2015, is available at https://fluxnet.org/data/fluxnet2015-dataset. All the data used in this study are available from their respective sources linked above.

Acknowledgments
The work was supported by the Strategic Priority Research Program of the Chinese Academy of Sciences (XDA28060200) and the 2115 Talent Development Program of China Agricultural University (00109016). We acknowledge all the producers of the datasets used in this study. We thank two anonymous reviewers for their constructive comments to further improve the quality of this manuscript.

References

Abatzoglou, J. T., Dobrowski, S. Z., Parks, S. A., & Hegewisch, K. C. (2018). TerraClimate, a high-resolution global dataset of monthly climate and climatic water balance from 1958–2015. *Scientific Data*, *5*, 170191. https://doi.org/10.1038/sdata.2017.191

Ahlstrom, A., Raupach, M. R., Schurgers, G., Smith, B., Arneth, A., Jung, M., et al. (2015). The dominant role of semi-arid ecosystems in the trend and variability of the land CO_2 sink. *Science*, *348*, 895–899. https://doi.org/10.1126/science.aaa1668

Allen, C. D., Breshears, D. D., & McDowell, N. G. (2015). On underestimation of global vulnerability to tree mortality and forest die-off from hotter drought in the Anthropocene. *Ecosphere*, *6*, art129. https://doi.org/10.1890/es15-00203.1

Baker, N. R. (2008). Chlorophyll fluorescence: A probe of photosynthesis in vivo. *Annual Review of Plant Biology*, *59*, 89–113. https://doi.org/10.1146/annurev.arplant.59.032607.092759

Bastos, A., Ciais, P., Chevallier, F., Rodenbeck, C., Ballantyne, A. P., Maignan, F., et al. (2019). Contrasting effects of CO_2 fertilization, land-use change and warming on seasonal amplitude of Northern Hemisphere CO_2 exchange. *Atmospheric Chemistry and Physics*, *19*, 12361–12375. https://doi.org/10.5194/acp-19-12361-2019

Bonan, G. B., Williams, M., Fisher, R. A., & Oleson, K. W. (2014). Modeling stomatal conductance in the Earth system: Linking leaf water-use efficiency and water transport along the soil-plant-atmosphere continuum. *Geoscientific Model Development*, *7*, 2193–2222. https://doi.org/10.5194/gmd-7-2193-2014

Breshears, D. D., Fontaine, J. B., Ruthrof, K. X., Field, J. P., Feng, X., Burger, J. R., et al. (2021). Underappreciated plant vulnerabilities to heat waves. *New Phytologist*, *231*, 32–39. https://doi.org/10.1111/nph.17348

Chen, A. N., Mao, J. F., Ricciuto, D., Xiao, J. F., Frankenberg, C., Li, X., et al. (2020). Moisture availability mediates the relationship between terrestrial gross primary production and solar-induced chlorophyll fluorescence: Insights from global-scale variations. *Global Change Biology*, *27*, 1144–1156. https://doi.org/10.1111/gcb.15373

Chen, C., Park, T., Wang, X. H., Piao, S. L., Xu, B. D., Chaturvedi, R. K., et al. (2019). China and India lead in greening of the world through land-use management. *Nature Sustainability*, *2*, 122–129. https://doi.org/10.1038/s41893-019-0220-7

Chen, T., de Jeu, R. A. M., Liu, Y. Y., van der Werf, G. R., & Dolman, A. J. (2014). Using satellite based soil moisture to quantify the water driven variability in NDVI: A case study over mainland Australia. *Remote Sensing of Environment*, *140*, 330–338. https://doi.org/10.1016/j.rse.2013.08.022

Dechant, B., Ryu, Y., Badgley, G., Zeng, Y. L., Berry, J. A., Zhang, Y. G., et al. (2020). Canopy structure explains the relationship between photosynthesis and sun-induced chlorophyll fluorescence in crops. *Remote Sensing of Environment*, *241*, 111733. https://doi.org/10.1016/j.rse.2020.111733

De Kauwe, M. G., Medlyn, B. E., Zaehle, S., Walker, A. P., Dietze, M. C., Wang, Y. P., et al. (2014). Where does the carbon go? A model-data intercomparison of vegetation carbon allocation and turnover processes at two temperate forest free-air CO_2 enrichment sites. *New Phytologist*, *203*, 883–899. https://doi.org/10.1111/nph.12847

De Sy, V., Herold, M., Achard, F., Beuchle, R., Clevers, J. G. P. W., Lindquist, E., & Verchot, L. (2015). Land use patterns and related carbon losses following deforestation in South America. *Environmental Research Letters*, *10*, 124004. https://doi.org/10.1088/1748-9326/10/12/124004

Ding, J. Z., Yang, T., Zhao, Y. T., Liu, D., Wang, X. Y., Yao, Y. T., et al. (2018). Increasingly important role of atmospheric aridity on Tibetan alpine grasslands. *Geophysical Research Letters*, *45*, 2852–2859. https://doi.org/10.1002/2017gl076803

Ding, Z., Peng, J., Qiu, S., & Zhao, Y. (2020). Nearly half of global vegetated area experienced inconsistent vegetation growth in terms of greenness, cover, and productivity. *Earth's Future*, *8*, e2020EF001618. https://doi.org/10.1029/2020ef001618

Doughty, C. E., Metcalfe, D. B., Girardin, C. A. J., Amezquita, F. F., Cabrera, D. G., Huasco, W. H., et al. (2015). Drought impact on forest carbon dynamics and fluxes in Amazonia. *Nature*, *519*, 78–82. https://doi.org/10.1038/nature14213

Falkowski, P., Scholes, R. J., Boyle, E., Canadell, J., Canfield, D., Elser, J., et al. (2000). The global carbon cycle: A test of our knowledge of Earth as a system. *Science*, *290*, 291–296. https://doi.org/10.1126/science.290.5490.291

Fernandez-Martinez, M., Sardans, J., Chevallier, F., Ciais, P., Obersteiner, M., Vicca, S., et al. (2019). Global trends in carbon sinks and their relationships with CO_2 and temperature. *Nature Climate Change*, *9*, 73–79. https://doi.org/10.1038/s41558-018-0367-7

Ficklin, D. L., & Novick, K. A. (2017). Historic and projected changes in vapor pressure deficit suggest a continental-scale drying of the United States atmosphere. *Journal of Geophysical Research: Atmospheres*, *122*, 2061–2079. https://doi.org/10.1002/2016jd025855

Field, C. B., Lobell, D. B., Peters, H. A., & Chiariello, N. R. (2007). Feedbacks of terrestrial ecosystems to climate change. *Annual Review of Environment and Resources*, *32*, 1–29. https://doi.org/10.1146/annurev.energy.32.053006.141119

Flexas, J., Escalona, J. M., Evain, S., Gulias, J., Moya, I., Osmond, C. B., & Medrano, H. (2002). Steady-state chlorophyll fluorescence (Fs) measurements as a tool to follow variations of net CO_2 assimilation and stomatal conductance during water-stress in C-3 plants. *Physiologia Plantarum*, *114*, 231–240. https://doi.org/10.1034/j.1399-3054.2002.1140209.x

Fournier, A., Daumard, F., Champagne, S., Ounis, A., Goulas, Y., & Moya, I. (2012). Effect of canopy structure on sun-induced chlorophyll fluorescence. *ISPRS Journal of Photogrammetry and Remote Sensing*, *68*, 112–120. https://doi.org/10.1016/j.isprsjprs.2012.01.003

Frankenberg, C., Fisher, J. B., Worden, J., Badgley, G., Saatchi, S. S., Lee, J. E., et al. (2011). New global observations of the terrestrial carbon cycle from GOSAT: Patterns of plant fluorescence with gross primary productivity. *Geophysical Research Letters*, *38*, L17706. https://doi.org/10.1029/2011gl048738

Friedlingstein, P., Jones, M. W., O'Sullivan, M., Andrew, R. M., Hauck, J., Peters, G. P., et al. (2019). Global carbon budget 2019. *Earth System Science Data*, *11*, 1783–1838. https://doi.org/10.5194/essd-11-1783-2019

Friedlingstein, P., Meinshausen, M., Arora, V. K., Jones, C. D., Anav, A., Liddicoat, S. K., & Knutti, R. (2014). Uncertainties in CMIP5 climate projections due to carbon cycle feedbacks. *Journal of Climate*, *27*, 511–526. https://doi.org/10.1175/jcli-d-12-00579.1

Fu, Z., Ciais, P., Prentice, I. C., Gentine, P., Makowski, D., Bastos, A., et al. (2022). Atmospheric dryness reduces photosynthesis along a large range of soil water deficits. *Nature Communications*, *13*, 989. https://doi.org/10.1038/s41467-022-28652-7

Gonsamo, A., Ciais, P., Miralles, D. G., Sitch, S., Dorigo, W., Lombardozzi, D., et al. (2021). Greening drylands despite warming consistent with carbon dioxide fertilization effect. *Global Change Biology*, *27*, 3336–3349. https://doi.org/10.1111/gcb.15658

Green, J. K., Berry, J., Ciais, P., Zhang, Y., & Gentine, P. (2020). Amazon rainforest photosynthesis increases in response to atmospheric dryness. *Science Advances*, *6*, abb7232. https://doi.org/10.1126/sciadv.abb7232

Grossiord, C., Buckley, T. N., Cernusak, L. A., Novick, K. A., Poulter, B., Siegwolf, R. T. W., et al. (2020). Plant responses to rising vapor pressure deficit. *New Phytologist*, *226*, 1550–1566. https://doi.org/10.1111/nph.16485

Gu, L. H., Han, J. M., Wood, J. D., Chang, C. Y. Y., & Sun, Y. (2019). Sun-induced Chl fluorescence and its importance for biophysical modeling of photosynthesis based on light reactions. *New Phytologist*, *223*, 1179–1191. https://doi.org/10.1111/nph.15796

Guanter, L., Zhang, Y. G., Jung, M., Joiner, J., Voigt, M., Berry, J. A., et al. (2014). Global and time-resolved monitoring of crop photosynthesis with chlorophyll fluorescence. *Proceedings of the National Academy of Sciences of the United States of America*, *111*, E1327–E1333. https://doi.org/10.1073/pnas.1320008111

Haverd, V., Smith, B., Canadell, J. G., Cuntz, M., Mikaloff-Fletcher, S., Farquhar, G., et al. (2020). Higher than expected CO_2 fertilization inferred from leaf to global observations. *Global Change Biology*, *26*, 2390–2402. https://doi.org/10.1111/gcb.14950

He, B., Chen, C., Lin, S., Yuan, W., Chen, H. W., Chen, D., et al. (2021). Worldwide impacts of atmospheric vapor pressure deficit on the interannual variability of terrestrial carbon sinks. *National Science Review*, *9*. https://doi.org/10.1093/nsr/nwab150

IPCC. (2018). *Global warming of 1.5°C. An IPCC Special Report on the impacts of global warming of 1.5°C above pre-industrial levels and related global greenhouse gas emission pathways, in the context of strengthening the global response to the threat of climate change, sustainable development, and efforts to eradicate poverty*. In the context of strengthening the global response.

Jacobson, A. R., Schuldt, K. N., Miller, J. B., Oda, T., Tans, P., Andrews, A., et al. (2020). *CarbonTracker CT2019B*. NOAA Global Monitoring Laboratory. http://dx.doi.org/10.25925/20201008

Jiao, W., Wang, L., Smith, W. K., Chang, Q., Wang, H., & D'Odorico, P. (2021). Observed increasing water constraint on vegetation growth over the last three decades. *Nature Communications*, *12*, 3777. https://doi.org/10.1038/s41467-021-24016-9

Jiao, W. Z., Chang, Q., & Wang, L. X. (2019). The sensitivity of satellite solar-induced chlorophyll fluorescence to meteorological drought. *Earth's Future*, *7*, 558–573. https://doi.org/10.1029/2018ef001087

Jung, M., Reichstein, M., Ciais, P., Seneviratne, S. I., Sheffield, J., Goulden, M. L., et al. (2010). Recent decline in the global land evapotranspiration trend due to limited moisture supply. *Nature*, *467*, 951–954. https://doi.org/10.1038/nature09396

Konings, A. G., & Gentine, P. (2017). Global variations in ecosystem-scale isohydricity. *Global Change Biology*, *23*, 891–905. https://doi.org/10.1111/gcb.13389

Le Quere, C., Raupach, M. R., Canadell, J. G., Marland, G., Bopp, L., Ciais, P., et al. (2009). Trends in the sources and sinks of carbon dioxide. *Nature Geoscience*, *2*, 831–836. https://doi.org/10.1038/ngeo689

Li, X., & Xiao, J. F. (2019). A global, 0.05-degree product of solar-induced chlorophyll fluorescence derived from OCO-2, MODIS, and reanalysis data. *Remote Sensing*, *11*, 517. https://doi.org/10.3390/rs11050517

Li, X., Xiao, J. F., He, B. B., Arain, M. A., Beringer, J., Desai, A. R., et al. (2018). Solar-induced chlorophyll fluorescence is strongly correlated with terrestrial photosynthesis for a wide variety of biomes: First global analysis based on OCO-2 and flux tower observations. *Global Change Biology*, *24*, 3990–4008. https://doi.org/10.1111/gcb.14297

Liu, L. B., Gudmundsson, L., Hauser, M., Qin, D. H., Li, S. C., & Seneviratne, S. I. (2020). Soil moisture dominates dryness stress on ecosystem production globally. *Nature Communications*, *11*, 4892. https://doi.org/10.1038/s41467-020-18631-1

Liu, Q., Piao, S. L., Janssens, I. A., Fu, Y. S., Peng, S. S., Lian, X., et al. (2018). Extension of the growing season increases vegetation exposure to frost. *Nature Communications*, *9*, 426. https://doi.org/10.1038/s41467-017-02690-y

Liu, X. P., Pei, F. S., Wen, Y. Y., Li, X., Wang, S. J., Wu, C. J., et al. (2019). Global urban expansion offsets climate-driven increases in terrestrial net primary productivity. *Nature Communications*, *10*, 5558. https://doi.org/10.1038/s41467-019-13462-1

Lopez, J., Way, D. A., & Sadok, W. (2021). Systemic effects of rising atmospheric vapor pressure deficit on plant physiology and productivity. *Global Change Biology*, *27*, 1704–1720. https://doi.org/10.1111/gcb.15548

Lu, X. L., Liu, Z. Q., An, S. Q., Miralles, D. G., Maes, W. H., Liu, Y. L., & Tang, J. W. (2018). Potential of solar-induced chlorophyll fluorescence to estimate transpiration in a temperate forest. *Agricultural and Forest Meteorology*, *252*, 75–87. https://doi.org/10.1016/j.agrformet.2018.01.017

Malhi, Y., Roberts, J. T., Betts, R. A., Killeen, T. J., Li, W. H., & Nobre, C. A. (2008). Climate change, deforestation, and the fate of the Amazon. *Science*, *319*, 169–172. https://doi.org/10.1126/science.1146961

Medlyn, B. E., De Kauwe, M. G., Zaehle, S., Walker, A. P., Duursma, R. A., Luus, K., et al. (2016). Using models to guide field experiments: A priori predictions for the CO_2 response of a nutrient- and water-limited native eucalypt woodland. *Global Change Biology*, *22*, 2834–2851. https://doi.org/10.1111/gcb.13268

Meng, X., Li, R., Luan, L., Lyu, S., Zhang, T., Ao, Y., et al. (2018). Detecting hydrological consistency between soil moisture and precipitation and changes of soil moisture in summer over the Tibetan Plateau. *Climate Dynamics*, *51*, 4157–4168. https://doi.org/10.1007/s00382-017-3646-5

Migliavacca, M., Perez-Priego, O., Rossini, M., El-Madany, T. S., Moreno, G., van der Tol, C., et al. (2017). Plant functional traits and canopy structure control the relationship between photosynthetic CO_2 uptake and far-red sun-induced fluorescence in a Mediterranean grassland under different nutrient availability. *New Phytologist*, *214*, 1078–1091. https://doi.org/10.1111/nph.14437

Myneni, R. B., Keeling, C. D., Tucker, C. J., Asrar, G., & Nemani, R. R. (1997). Increased plant growth in the northern high latitudes from 1981 to 1991. *Nature*, *386*, 698–702. https://doi.org/10.1038/386698a0

Nandintsetseg, B., & Shinoda, M. (2014). Multi-decadal soil moisture trends in Mongolia and their relationships to precipitation and evapotranspiration. *Arid Land Research and Management*, *28*, 247–260. https://doi.org/10.1080/15324982.2013.861882

Nemani, R. R., Keeling, C. D., Hashimoto, H., Jolly, W. M., Piper, S. C., Tucker, C. J., et al. (2003). Climate-driven increases in global terrestrial net primary production from 1982 to 1999. *Science*, *300*, 1560–1563. https://doi.org/10.1126/science.1082750

Novick, K. A., Ficklin, D. L., Stoy, P. C., Williams, C. A., Bohrer, G., Oishi, A. C., et al. (2016). The increasing importance of atmospheric demand for ecosystem water and carbon fluxes. *Nature Climate Change*, *6*, 1023–1027. https://doi.org/10.1038/nclimate3114

Pastorello, G., Trotta, C., Canfora, E., Chu, H., Christianson, D., Cheah, Y.-W., et al. (2020). The FLUXNET2015 dataset and the ONEFlux processing pipeline for eddy covariance data. *Scientific Data*, *7*, 225. https://doi.org/10.1038/s41597-020-0534-3

Penuelas, J., Ciais, P., Canadell, J. G., Janssens, I. A., Fernandez-Martinez, M., Carnicer, J., et al. (2017). Shifting from a fertilization-dominated to a warming-dominated period. *Nature Ecology & Evolution*, *1*, 1438–1445. https://doi.org/10.1038/s41559-017-0274-8

Piao, S. L., Friedlingstein, P., Ciais, P., Viovy, N., & Demarty, J. (2007). Growing season extension and its impact on terrestrial carbon cycle in the Northern Hemisphere over the past 2 decades. *Global Biogeochemical Cycles*, *21*, GB3018. https://doi.org/10.1029/2006gb002888

Piao, S. L., Liu, Q., Chen, A. P., Janssens, I. A., Fu, Y. S., Dai, J. H., et al. (2019). Plant phenology and global climate change: Current progresses and challenges. *Global Change Biology*, *25*, 1922–1940. https://doi.org/10.1111/gcb.14619

Piao, S. L., Sitch, S., Ciais, P., Friedlingstein, P., Peylin, P., Wang, X. H., et al. (2013). Evaluation of terrestrial carbon cycle models for their response to climate variability and to CO_2 trends. *Global Change Biology*, *19*, 2117–2132. https://doi.org/10.1111/gcb.12187

Piao, S. L., Yin, G. D., Tan, J. G., Cheng, L., Huang, M. T., Li, Y., et al. (2015). Detection and attribution of vegetation greening trend in China over the last 30 years. *Global Change Biology*, *21*, 1601–1609. https://doi.org/10.1111/gcb.12795

Porcar-Castell, A., Tyystjarvi, E., Atherton, J., van der Tol, C., Flexas, J., Pfundel, E. E., et al. (2014). Linking chlorophyll a fluorescence to photosynthesis for remote sensing applications: Mechanisms and challenges. *Journal of Experimental Botany*, *65*, 4065–4095. https://doi.org/10.1093/jxb/eru191

Randerson, J. T., Thompson, M. V., Conway, T. J., Fung, I. Y., & Field, C. B. (1997). The contribution of terrestrial sources and sinks to trends in the seasonal cycle of atmospheric carbon dioxide. *Global Biogeochemical Cycles*, *11*, 535–560. https://doi.org/10.1029/97gb02268

Reichstein, M., Falge, E., Baldocchi, D., Papale, D., Aubinet, M., Berbigier, P., et al. (2005). On the separation of net ecosystem exchange into assimilation and ecosystem respiration: Review and improved algorithm. *Global Change Biology*, *11*, 1424–1439. https://doi.org/10.1111/j.1365-2486.2005.001002.x

Restaino, C. M., Peterson, D. L., & Littell, J. (2016). Increased water deficit decreases Douglas fir growth throughout Western US forests. *Proceedings of the National Academy of Sciences of the United States of America*, *113*, 9557–9562. https://doi.org/10.1073/pnas.1602384113

Rifai, S. W., De Kauwe, M. G., Ukkola, A. M., Cernusak, L. A., Meir, P., Medlyn, B. E., & Pitman, A. J. (2022). Thirty-eight years of CO_2 fertilization has outpaced growing aridity to drive greening of Australian woody ecosystems. *Biogeosciences*, *19*, 491–515. https://doi.org/10.5194/bg-19-491-2022

Ryu, Y., Berry, J. A., & Baldocchi, D. D. (2019). What is global photosynthesis? History, uncertainties and opportunities. *Remote Sensing of Environment*, *223*, 95–114. https://doi.org/10.1016/j.rse.2019.01.016

Saatchi, S., Asefi-Najafabady, S., Malhi, Y., Aragao, L. E. O. C., Anderson, L. O., Myneni, R. B., & Nemani, R. (2013). Persistent effects of a severe drought on Amazonian forest canopy. *Proceedings of the National Academy of Sciences of the United States of America*, *110*, 565–570. https://doi.org/10.1073/pnas.1204651110

Schimel, D., Stephens, B. B., & Fisher, J. B. (2015). Effect of increasing CO_2 on the terrestrial carbon cycle. *Proceedings of the National Academy of Sciences of the United States of America*, *112*, 436–441. https://doi.org/10.1073/pnas.1407302112

Shan, N., Zhang, Y. G., Chen, J. M., Ju, W. M., Migliavacca, M., Penuelas, J., et al. (2021). A model for estimating transpiration from remotely sensed solar-induced chlorophyll fluorescence. *Remote Sensing of Environment*, *252*, 112134. https://doi.org/10.1016/j.rse.2020.112134

Smith, W. K., Reed, S. C., Cleveland, C. C., Ballantyne, A. P., Anderegg, W. R. L., Wieder, W. R., et al. (2016). Large divergence of satellite and Earth system model estimates of global terrestrial CO_2 fertilization. *Nature Climate Change*, *6*, 306–310. https://doi.org/10.1038/nclimate2879

Song, Y., Wang, L., & Wang, J. (2021). Improved understanding of the spatially-heterogeneous relationship between satellite solar-induced chlorophyll fluorescence and ecosystem productivity. *Ecological Indicators*, *129*, 107949. https://doi.org/10.1016/j.ecolind.2021.107949

Sun, Y., Frankenberg, C., Wood, J. D., Schimel, D. S., Jung, M., Guanter, L., et al. (2017). OCO-2 advances photosynthesis observation from space via solar-induced chlorophyll fluorescence. *Science*, *358*, eaam5747. https://doi.org/10.1126/science.aam5747

Thomas, R. T., Prentice, L. C., Graven, H., Ciais, P., Fisher, J. B., Hayes, D. J., et al. (2016). Increased light-use efficiency in northern terrestrial ecosystems indicated by CO_2 and greening observations. *Geophysical Research Letters*, *43*, 11339–11349. https://doi.org/10.1002/2016gl070710

van der Tol, C., Berry, J. A., Campbell, P. K. E., & Rascher, U. (2014). Models of fluorescence and photosynthesis for interpreting measurements of solar-induced chlorophyll fluorescence. *Journal of Geophysical Research: Biogeosciences*, *119*, 2312–2327. https://doi.org/10.1002/2014jg002713

Wang, S. H., Zhang, Y. G., Ju, W. M., Chen, J. M., Ciais, P., Cescatti, A., et al. (2020). Recent global decline of CO_2 fertilization effects on vegetation photosynthesis. *Science*, *370*, 1295–1300. https://doi.org/10.1126/science.abb7772

Wang, S. H., Zhang, Y. G., Ju, W. M., Qiu, B., & Zhang, Z. Y. (2021). Tracking the seasonal and inter-annual variations of global gross primary production during last four decades using satellite near-infrared reflectance data. *Science of the Total Environment*, *755*, 142569. https://doi.org/10.1016/j.scitotenv.2020.142569

Wang, X. F., Xiao, J. F., Li, X., Cheng, G. D., Ma, M. G., Zhu, G. F., et al. (2019). No trends in spring and autumn phenology during the global warming hiatus. *Nature Communications*, *10*, 2389. https://doi.org/10.1038/s41467-019-10235-8

Wang, X. H., Piao, S. L., Ciais, P., Friedlingstein, P., Myneni, R. B., Cox, P., et al. (2014). A two-fold increase of carbon cycle sensitivity to tropical temperature variations. *Nature*, *506*, 212–215. https://doi.org/10.1038/nature12915

Willett, K. M., Dunn, R. J. H., Thorne, P. W., Bell, S., de Podesta, M., Parker, D. E., et al. (2014). HadISDH land surface multi-variable humidity and temperature record for climate monitoring. *Climate of the Past*, *10*, 1983–2006. https://doi.org/10.5194/cp-10-1983-2014

Winkler, A. J., Myneni, R. B., Hannart, A., Sitch, S., Haverd, V., Lombardozzi, D., et al. (2021). Slowdown of the greening trend in natural vegetation with further rise in atmospheric CO_2. *Biogeosciences*, *18*, 4985–5010. https://doi.org/10.5194/bg-18-4985-2021

Xia, J. Y., Chen, J. Q., Piao, S. L., Ciais, P., Luo, Y. Q., & Wan, S. Q. (2014). Terrestrial carbon cycle affected by non-uniform climate warming. *Nature Geoscience*, *7*, 173–180. https://doi.org/10.1038/ngeo2093

Xiao, J. F., Chevallier, F., Gomez, C., Guanter, L., Hicke, J. A., Huete, A. R., et al. (2019). Remote sensing of the terrestrial carbon cycle: A review of advances over 50 years. *Remote Sensing of Environment*, *233*, 111383. https://doi.org/10.1016/j.rse.2019.111383

Yuan, W. P., Liu, S. G., Yu, G. R., Bonnefond, J. M., Chen, J. Q., Davis, K., et al. (2010). Global estimates of evapotranspiration and gross primary production based on MODIS and global meteorology data. *Remote Sensing of Environment*, *114*, 1416–1431. https://doi.org/10.1016/j.rse.2010.01.022

Yuan, W. P., Zheng, Y., Piao, S. L., Ciais, P., Lombardozzi, D., Wang, Y. P., et al. (2019). Increased atmospheric vapor pressure deficit reduces global vegetation growth. *Science Advances*, *5*, eaax1396. https://doi.org/10.1126/sciadv.aax1396

Zhang, Y., Joiner, J., Alemohammad, S. H., Zhou, S., & Gentine, P. (2018). A global spatially contiguous solar-induced fluorescence (CSIF) dataset using neural networks. *Biogeosciences*, *15*, 5779–5800. https://doi.org/10.5194/bg-15-5779-2018

Zhang, Y., Xiao, X., Wu, X., Zhou, S., Zhang, G., Qin, Y., & Dong, J. (2017). A global moderate resolution dataset of gross primary production of vegetation for 2000–2016. *Scientific Data*, *4*, 170165. https://doi.org/10.1038/sdata.2017.165

Zhang, Y. G., Guanter, L., Berry, J. A., Joiner, J., van der Tol, C., Huete, A., et al. (2014). Estimation of vegetation photosynthetic capacity from space-based measurements of chlorophyll fluorescence for terrestrial biosphere models. *Global Change Biology*, *20*, 3727–3742. https://doi.org/10.1111/gcb.12664

Zhang, Y. L., Song, C. H., Band, L. E., Sun, G., & Li, J. X. (2017). Reanalysis of global terrestrial vegetation trends from MODIS products: Browning or greening? *Remote Sensing of Environment*, *191*, 145–155. https://doi.org/10.1016/j.rse.2016.12.018

Zhu, Z. C., Piao, S. L., Myneni, R. B., Huang, M. T., Zeng, Z. Z., Canadell, J. G., et al. (2016). Greening of the Earth and its drivers. *Nature Climate Change*, *6*, 791–795. https://doi.org/10.1038/nclimate3004